

Dynamical study of the structural and magnetic phases in Pr_2NiO_4 single crystals by Raman spectroscopy

A. de Andrés and J. L. Martínez

Instituto de Ciencia de Materiales de Madrid, Consejo Superior de Investigaciones Científicas, Universidad Autónoma de Madrid, Departamento de Física Aplicada C-IV, Madrid E-28049, Spain

P. Odier

Centre de Physique des Hautes Températures, Centre National de la Recherche Scientifique F-45071, Orleans CEDEX 2, France

(Received 13 December 1991)

Polarized Raman spectra of stoichiometric Pr_2NiO_4 single crystals have been obtained for temperatures between 74 and 300 K in a spectral range of 6000 cm^{-1} . The lattice dynamics of the orthorhombic-to-tetragonal low-temperature phase transition has been characterized. The intensity associated with the in-plane Ni-O(1) modes is much lower than the corresponding modes related to motions along the c axis. Five A_g modes have been identified with the corresponding atomic vibrations. The frequencies and widths of some particular modes show a discontinuous behavior at the transition temperature ($T_c \approx 117\text{ K}$). Below this temperature, additional modes appear with very low intensities. Polarized two-magnon scattering is observed as wide bands whose intensity increases with decreasing temperature as does the magnetization. The characteristics of the observed two-magnon spectra do not correspond to classical two-spin scattering; their selection rules indicate that the Ni interlayer coupling plays an important role in the process.

I. INTRODUCTION

The lattice dynamics of superconducting rare-earth cuprates has been widely studied by Raman^{1,2} and infrared (ir) spectroscopies^{3,4} and by neutron scattering.^{5,6} Nickel oxides with similar crystal structure have revealed many important similarities and some differences in relation with their electronic properties and the detailed structure of these materials. Rare-earth nickelates present striking complex behavior, depending on the oxygen stoichiometry, and so it then becomes necessary to have precise control over this parameter, which determines the crystal structure of the sample and many of the magnetic and transport properties.

The study of the lattice dynamics of structurally well characterized nickelates has only recently been initiated; among these, the $\text{La}_2\text{NiO}_{4+\delta}$ compound has been the most widely studied. The ir and Raman spectroscopies,⁷⁻⁹ together with the neutron scattering and normal-mode dispersion curve calculations,^{10,11} have clarified the dynamics of the phase transitions in this system. Recently, similar studies have been conducted on $R_2\text{NiO}_{4+\delta}$ ($R = \text{La, Pr, and Nd}$) ceramic samples with controlled stoichiometry and structure by use of Raman (Refs. 12 and 13) and ir (Ref. 14) spectroscopies. The availability of single crystals allows a deeper study in this field. Another interesting subject is the observation in these compounds, by Raman techniques, of the collective spin modes in their antiferromagnetic phases. Two-magnon light scattering has been detected in some cuprates $R_2\text{CuO}_4$ [$R = \text{La, Nd, Pr, and Sm}$ (Refs. 15-17)]

and in La_2NiO_4 (Ref. 16).

Pr_2NiO_4 , in the stoichiometric composition ($\delta = 0$), is orthorhombic at room temperature (commonly called low-temperature orthorhombic, LTO) with space group $Bmab$. It undergoes a structural phase transition (at 117 K) to the tetragonal $P4_2/nm$ structure^{18,19} (low-temperature tetragonal, LTT). Another phase transition is expected, at high temperatures, to the usual K_2NiF_4 tetragonal structure (high-temperature tetragonal, HTT) of the superconductor La_2CuO_4 compounds.

The magnetic structure of this compound also presents a complex behavior. The Ni ions order antiferromagnetically at $T_{N_1} = 325\text{ K}$ with a propagation vector $\mathbf{k} = (1, 0, 0)$ and the magnetic moments along the a axis. This system shows, as the related cuprates, a square planar lattice of nickel spins coupled by superexchange through the oxygen ions. The net staggered magnetization increases on decreasing the temperature, reaching its maximum value around 150 K, where the saturation moment of Ni is achieved ($1.6\mu_B$). At the structural phase transition the Ni spin reorientates in the a - b plane and the coexistence of the LTO and LTT phases occurs associated with the strong first-order character of the structural transformation.¹⁹ At $T_{N_2} = 90\text{ K}$ a magnetic phase transition takes place to a different magnetic order for the Ni sublattice. This phase is mainly characterized by a strong out-of-plane spin component ordered antiferromagnetically along the c axis.²⁰

The aim of this research is to compare the nickelates with related high- T_c superconductor cuprates through

the information obtained by light-scattering techniques. It is also interesting by itself because of the strong correlation of the static structure and lattice dynamics with the transport and magnetic properties.

The rest of this paper is organized as follows: We briefly describe the experimental setup and crystal growth procedure; then the different crystal structures and phase transitions for this compound together with the corresponding normal-mode analysis are commented upon. In the fourth part, a description of the magnetic structures and recent theories for two-magnon light scattering, in this kind of system is given. The fifth section, which contains the results and discussion, is subdivided into two parts: The first part deals with the lattice vibration modes and the structural phase transitions and the second part, with two-magnon light scattering through the different magnetic order.

II. EXPERIMENTAL

The $\text{Pr}_2\text{NiO}_{4+\delta}$ samples were grown with the floating-zone method with a CO_2 laser. The nickel to praseodymium ratio is very close to 2; however, there is an oxygen excess, which stays as a defect in the structure. A reduction process at 470 K in an Ar flow during 10 h is enough to force the sample to attain the stoichiometric value of $\delta=0$, demonstrated by a structural comparison. The crystals used in these experiments are small cubes of size around 1 mm^3 taken from a batch of size about 260 mm^3 .

Raman-scattering experiments have been performed with an X - Y Dilor multichannel spectrometer, the excitation source being a Spectra Physics Ar^+ laser. The samples were located inside an Oxford Instruments cryostat chamber with helium exchange gas, the temperature was varied from 300 to 74 K, and a spectral range of around 6000 cm^{-1} has been scanned. We have used the 5145- and $4880\text{-}\text{\AA}$ lines of the laser and the beam power on the sample was 20 mW or less. The low intensity avoids possible sample overheating.

The spectra were recorded in the backscattering geometry and the polarizations of the incident and scattered beams were analyzed. The notation used here, (ab) , indicates the polarizations of the incident (a) and the scattered beam (b) in the axes of the crystal. The obtained spectra were normalized by the spectral response of the spectrometer for the two different polarizations: parallel and perpendicular to the slits. This normalization is important, especially when a very wide frequency range is recorded and when polarized spectra are compared. The strong variation of the spectrometer sensibility with the scattered-light wavelength and with its polarization produces strong differences in the signal-to-noise ratio that can be observed in the presented results.

III. CRYSTAL STRUCTURES AND NORMAL MODES

It is now well known that both the structure and properties of these oxides depend strongly on the deviation from stoichiometry, present as an excess in oxygen content. The samples studied here have been previously carefully structurally and magnetically characterized by means of high-resolution neutron-diffraction and bulk

magnetization measurements.^{18–20}

The room-temperature structure is the orthorhombic $Bmab$ space group with $Z=2$ (LTO) (the lattice parameters are given in Table I). The measurement of the orthorhombic strain parameter $[2(b-a)/(a+b)]$ versus temperature gives, by extrapolation, an estimation of the LTO-to-HTT phase-transition temperature of 1500 K.¹⁹ Nevertheless this phase transition has not yet been observed because its temperature is quite high. Note the enormous difference in the HTT-to-LTO transition temperature between the La oxides (770 K for the nickelate and 530 K for the cuprate¹) and the unfilled $4f$ rare-earth oxides (the estimation for the Nd_2NiO_4 is 1900 K). The reason for this rests in the smaller size of the rare-earth ions (from La to Nd), which implies a mismatch between the NiO_2 and R_2O_2 layers. In order to accommodate each other, the system rotates the oxygen octahedron around the Ni ion and undergoes a phase transition from the ideal tetragonal structure to the orthorhombic one. The mechanism of this phase transition has been observed and described in different isostructural systems such as La_2CuO_4 and La_2NiO_4 . It is quite clear that it is a second-order transition driven by a soft mode as observed by neutron scattering.^{5,6}

A second-phase transition is present in Pr_2NiO_4 at 117 K to another tetragonal structure (LTT) ($P4_2/ncm$). This transition has been found to be first order. This could be expected because the LTT group is not a subgroup of the LTO group, and the transition cannot be carried out by softening a normal mode. In powder samples, it has been found that the two phases (LTO and LTT) coexist in the interval of temperatures between 100 and 125 K.¹⁹ Figure 1 shows, on the left-hand side, the structure of the HTT phase and, on the right-hand side, the ionic displacements needed to reach the two "low"-temperature phases (HHT \rightarrow LTO and HHT \rightarrow LTT). The Ni-O(1) and Pr-O(2) layers are distorted in a similar way in both low-temperature phases with respect to the perfect $I4/mmm$ structure. The differences arise from the axis of rotation of the oxygen octahedra: While in the LTO structure it is the a axis; in the LTT it is the $a+b$ axis. This change will have important effects in the magnetic structure.

TABLE I. Cell parameters and relevant interatomic distances (in \AA) of the two low-temperature phases (LTO and LTT).

	330 K <i>Bmab</i>	67 K <i>P4₂/ncm</i>
Pr_2NiO_4		
a (\AA)	5.4104	5.4920
b (\AA)	5.5824	
c (\AA)	12.2347	12.157
Ni-O(1)	1.954	1.945
Ni-O(1)'		1.974
Ni-O(2)	2.22	2.21
Pr-O(1)	2.50	2.44
Pr-O(1)'		2.57
Pr-O(2)	2.30	2.28

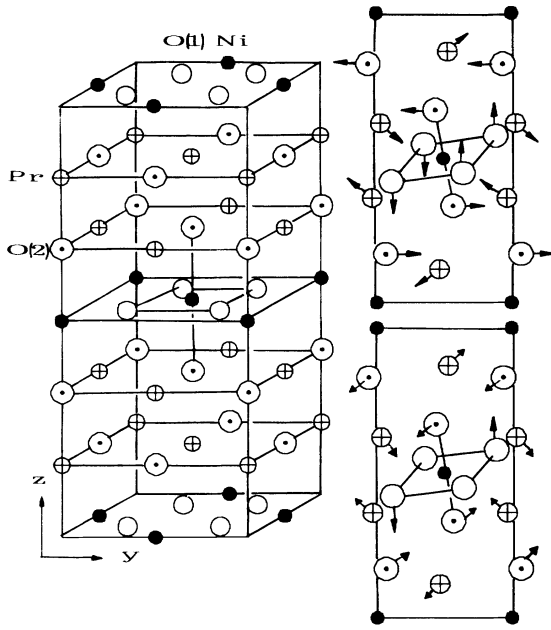


FIG. 1. On the left, the HTT structure with $Z=4$ is drawn. On the right, the atomic displacements needed to reach the two low-temperature phases (LTO and LTT) are shown. The primitive cell of the orthorhombic phase ($Bmab$) has $Z=2$ and contains only the ions printed in the right part.

A factor-group analysis of the low-temperature tetragonal and orthorhombic structures, together with the atomic movements of the Raman active modes, is given in Ref. 12. The high-temperature tetragonal phase (HTT) with the $I4/mmm$ space group and $Z=1$ has only 2 $A_g + 2 B_g$ Raman-active modes corresponding only to motions of the O(2) and Pr ions. The point group of the LTO structure at room temperature is D_{2h} , and its primitive cell contains 14 ions and 42 normal modes. The Ni ions are surrounded by distorted oxygen octahedra, and their site symmetry is C_{2h} , which has inversion symmetry so that the Ni ions are not involved in any Raman mode. The O(1) ions are no longer located at inversion centers, and so they contribute to some of the Raman modes. The irreducible representations of the 18 even Raman-active modes at $\mathbf{k}=0$ are $5 A_g + 3 B_{1g} + 4 B_{2g} + 6 B_{3g}$.

The low-temperature tetragonal structure (LTT) has a more symmetric point group (D_{4h}), but its primitive cell is doubled so that it contains 4 formula units and thus 28 ions and 84 normal modes. The 23 Raman active modes at the Γ point of the tetragonal group D_{4h} (Ref. 16) are $5 A_{1g} + 3 B_{1g} + 5 B_{2g} + 10 E_g$, the even A_{2g} modes being silent. The site symmetry of the Ni ions remains to be C_{2h} , but the four oxygens O(1) in the Ni plane are no longer equivalent; they have been called O(1) and O(1').

The eigenmodes of a crystal are linear combinations of the normal modes of the same symmetry, and the only reliable way to obtain them is through a dynamical-matrix reduction. We have used the force constants obtained in a previous work¹⁰ on similar compounds to estimate the actual vibration modes. Figure 2 shows six of the atomic

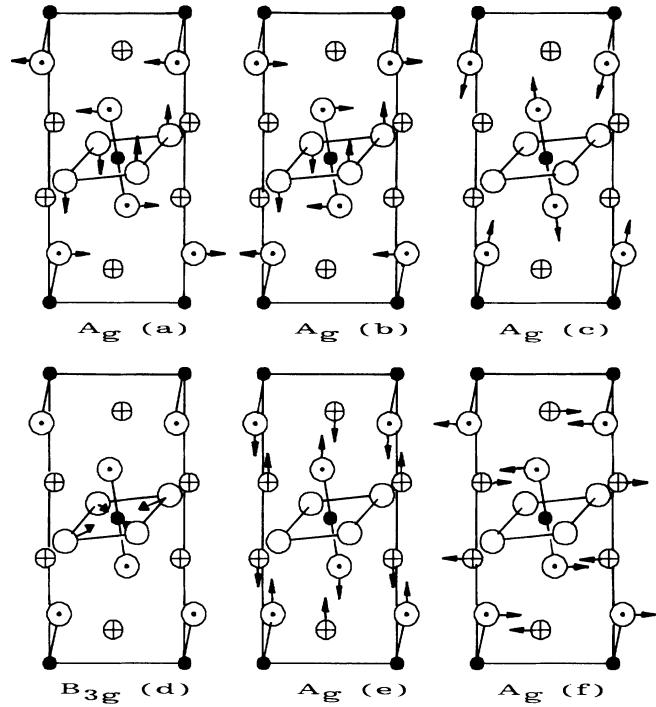


FIG. 2. The five A_g eigenmodes and the highest-frequency mode of B_{3g} symmetry of the $Bmab$ phase.

displacements of the LTO phase eigenmodes (the ions shown are those of the primitive cell).

IV. MAGNETIC STRUCTURE AND MAGNONS

The magnetic structure is, as stated before, quite complex. The interesting and differentiating point of Pr_2NiO_4 is the canting of the nickel magnetic moments at low temperatures. The magnetic moment of these ions has an out-of-plane component parallel to the z axis, which is very strong and is antiferromagnetically ordered in this direction as well as in the NiO_2 planes.

Towards the end of the 1960s, important experimental and theoretical work on magnons in antiferromagnetic (AFM) materials with the perovskite structure was done. Parkinson's theory²¹ predicted the correct shape for two-magnon Raman scattering in two-dimensional AFM systems with the K_2NiF_4 structure (the same as we have called HTT here). The magnetic Hamiltonian contains exchange interactions and anisotropy terms. Only one exchange J parameter was used, which describes the interaction between Ni ions in nearest-neighbor positions in the NiO_2 layers. The exchange between layers was considered to be an order of magnitude smaller: The ratio between the interlayer and intralayer Ni nearest-neighbor distances is about 1.9 for K_2NiF_4 . The anisotropy part of the Hamiltonian contains crystal-field terms and dipole-dipole terms, which, in these Ni compounds, are small compared with the exchange terms. The magnetic Hamiltonian then reduces to

$$H^{\text{mag}} = J_i \sum_j \mathbf{S}_i \cdot \mathbf{S}_j ,$$

and the magnon energies are given by

$$E_k^2 = (JSZ)^2 - (JSZ\gamma_k)^2, \quad \gamma_k = \frac{1}{2}[\cos(ak_x) - \cos(ak_y)],$$

where $Z (=4)$ is the number of nearest neighbors; k_x and k_y are the in-plane components of the magnon momentum (for the $K_2\text{NiF}_4$ structure).

The magnon density of states is limited to an energy interval and presents a maximum at the high-energy limit, which corresponds to the zone boundary (short wavelength) spin waves. The Raman Hamiltonian, which involves the creation of two magnons, when the interaction between these magnons is introduced and once it is simplified by symmetry considerations, is given by

$$H^{\text{Raman}} = A_i \Sigma_j (\mathbf{E}_1 \sigma_{ij}) \cdot (\mathbf{E}_2 \sigma_{ij}) \mathbf{S}_i \cdot \mathbf{S}_j,$$

where σ_{ij} are unit vectors connecting the i and j Ni ions in nearest-neighbor positions with opposite spins (\mathbf{S}_i and \mathbf{S}_j), and $\mathbf{E}_1, \mathbf{E}_2$ are the electric field vectors of the incoming and outgoing light.

The attractive interaction between the magnons decreases the energy of the processes, and so the shape of the observed band in light scattering differs from the joint density of states shifting the band maximum to lower values. For spin $\frac{1}{2}$, Parkinson's theory predicts a maximum at $2.7J$ and a cutoff (upper limit) at $4J$. For spin 1, the values are $6.8J$ and $8J$, respectively. The width of the band is around 11% of the energy at the band maximum.²¹ To date this theory fits the spectra observed in several nickelates as $K_2\text{NiF}_4$ (Ref. 22) or La_2NiO_4 (Ref. 16) well.

Recent works on cuprates¹⁵⁻¹⁷ ($R_2\text{CuO}_4$, $R = \text{La, Nd, Pr, Sm}$) have revealed quite different features of the two-magnon bands compared with the nickelates: The width is much larger, the intensity is important over the cutoff limit, and two-magnon bands of forbidden A_{1g} and B_{2g} symmetry are observed. There is then a difference because of the change from copper to nickel, which lies on the different spin values ($\frac{1}{2}$ to 1). Singh and co-workers^{23,24} have included, for the cuprates, quantum-spin fluctuations in the Heisenberg AFM ground state in order to explain the width of the observed two-magnon scattering from the spin flip of two Cu nearest neighbors in the xy plane. Moreover, these fluctuations allow different kinds of two-magnon processes in which the involved Cu moments are next-nearest neighbors. These processes would otherwise be forbidden because they do not conserve spin (the spins of these two Cu atoms are parallel). These authors have calculated the spectral moments (or cumulants), and so it is possible to compare them to the extracted one from the experimental curves using

$$M_1 = (\int \omega I(\omega) d\omega) / I_T, \quad \text{where } I_T = \int I(\omega) d\omega$$

and, for $n > 1$,

$$(M_n)^n = (\int (\omega - M_1)^n I(\omega) d\omega) / I_T.$$

In this case the predictions for $S = \frac{1}{2}$ are $M_1/J = 3.6$, $M_2/M_1 = 0.23$ (instead of 0.11), and $M_3/M_1 = 0.27$ (instead of 0.06).^{23,24}

V. EXPERIMENTAL RESULTS AND DISCUSSION

A. Structural phase transitions

Even if the HTT phase cannot be observed, it is very useful to take it into account in order to understand the dynamical properties of those compounds. All the different structures are slight distortions of this high-symmetry tetragonal one. The two transitions are accomplished by doubling the primitive cell (from $Z=1$ to 2 and to 4) by successive foldings of the Brillouin zone.

The correspondence between the modes of the two low-temperature phases (LTO to LTT) is as follows: A_g to A_{1g} , B_{1g} to A_{2g} (inactive), $1 A_g + 1 B_{1g}$ to $1 B_{1g} + 1 B_{2g}$, and $1 B_{2g} + 1 B_{3g}$ to $1 E_g$.

Figure 3 shows the spectra of a Pr_2NiO_4 stoichiometric single crystal at (a) 230 K and (b) 75 K (above and below the LTO to LTT phase transition temperature). The exciting wavelength was 4888 Å. In this configuration we obtain the (zz) components of the polarizability tensor derivatives of the different modes and, in this case, only the A_g modes must be observed. Notice that the number of expected modes is five A_g for the two phases. The upper part of Fig. 4 gives the (xy), (xx), and (yy) components for the same two temperatures as in Fig. 3. Here the observable modes are, in the orthorhombic phase, $5 A_g + 3 B_{1g}$ modes and, in the tetragonal (LTT) phase, the $5 A_g + 3 B_{1g} + 5 B_{2g}$ ones (five more). The lower part of the figure should give the (zx) and (zy) components of the polarizability derivative tensor. $4 B_{2g} + 6 B_{3g}$ modes are expected for the higher temperature, while ten E_g modes should appear at 75 K, and so the total number of modes is invariant. The collected spectra at the three different configurations are directly comparable after correcting

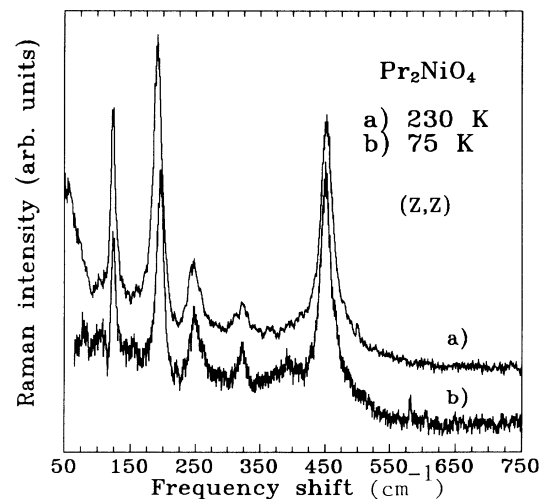


FIG. 3. Raman spectra of stoichiometric Pr_2NiO_4 single crystals at temperatures above and below the low-temperature structural phase transition ($T_c = 117$ K). The notation (zz) indicates the polarization of the incident and scattered electric fields. The a spectrum has been shifted upwards for clarity. Incident wavelength: 4880 Å.

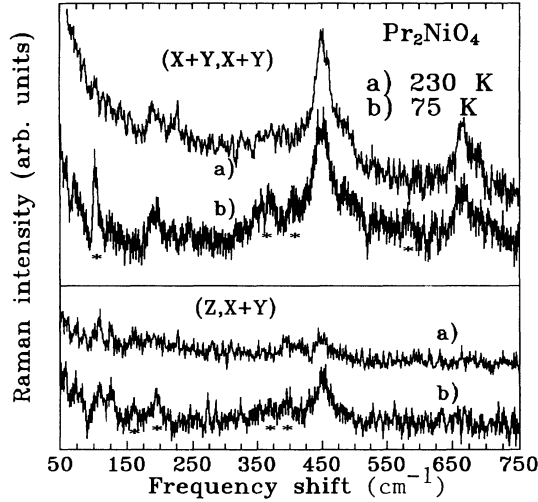


FIG. 4. Raman spectra of stoichiometric Pr_2NiO_4 single crystals at temperatures below and above the low-temperature structural phase transition. The intensity axis is expanded 1.6 times in comparison with that of Fig. 3. The upper part shows the $(x+y, x+y)$ configuration and the lower part the $(z, x+y)$ one. The stars indicates the new small peaks that appears below the phase transition. Incident wavelength: 4880 Å.

for the spectral response of the spectrometer. In order to compare the spectra at different temperatures, we have normalized them to the 450-cm^{-1} peak intensity.

The first striking feature is the difference in the peak intensities between the (zz) configuration and the other two. Strong intensities are expected for O(1) modes in the Ni-O(1) planes, which are of B_{3g} and B_{2g} symmetries and should appear in the lower part of Fig. 4. Nevertheless, in this geometry the measured scattered intensities are very low through the frequency range under study.

The high- and low-temperature spectra in Fig. 3 show the five A_g expected peaks. The weak peak labeled with an asterisk at 392 cm^{-1} at 75 K is not always observed, and so we will not take it into account. The low-frequency region (below 70 cm^{-1}) depends strongly on the focusing; so, even if some structure could be seen when it is observed in detail, we would not consider it. Basically, then, the two spectra are identical except for the shape and positions of some peaks, this will be commented upon below in some detail.

In the 230 K $(x+y, x+y)$ spectrum only three peaks are observed. In this configuration the (xx) and (yy) components of the five A_g modes together with the three B_{1g} modes are expected. On lowering the temperature five additional modes are predicted by group theory, and some additional weak peaks actually appear (marked with asterisks). Notice that the highest-frequency mode at 665 cm^{-1} is observed only in this configuration.

Finally, in the $(z, x+y)$ spectra, out of the ten expected modes only four can be detected as very weak peaks. At low temperature the intensities are slightly higher and two additional modes are observed. The observed peak frequencies for each geometry and temperature are listed in Table II.

TABLE II. Observed phonon frequencies (in cm^{-1}) at three different configurations for the LTO and LTT phases measured at 230 and 75 K, respectively.

(zz)		(xx, yy, xy)		(zx, zy)	
230 K	75 K	230 K	75 K	230 K	75 K
A_g	A_{1g}	$A_g + B_{1g}$	$A_{1g} + B_{1g} + B_{2g}$	$B_{2g} + B_{3g}$	E_g
	80				80
(102)	(103)		102	108	109
122	124			125	125
	(155)				159
190	194	191	192		196
246	249	223	243		
321	321		358		367
			406	406	394
451	450	451	448	447	451
		665	665		

The assignment of the detected modes in the orthorhombic phase has been done in the following way: The highest-frequency mode (665 cm^{-1}) must correspond to the shortest bond of the lightest atom, the O(1) stretching mode [Fig. 2(f)], which is of B_{3g} symmetry. Because of its symmetry, it must be observable only in the $(z, x+y)$ spectrum instead of the $(x+y, x+y)$ spectrum, but, even though the selection rules do not correspond to the expected ones for the scattering perpendicular to the c axis, the observed peaks are strongly polarized.

In the (zz) spectrum, we can separate the five A_g modes in two groups according to their behavior with temperature. Figure 5 plots the frequency versus temperature of four A_g modes. While the peaks at 125, 322 (not shown), and 450 cm^{-1} have frequencies nearly independent of temperature (as the B_{3g} mode at 665 cm^{-1}), the

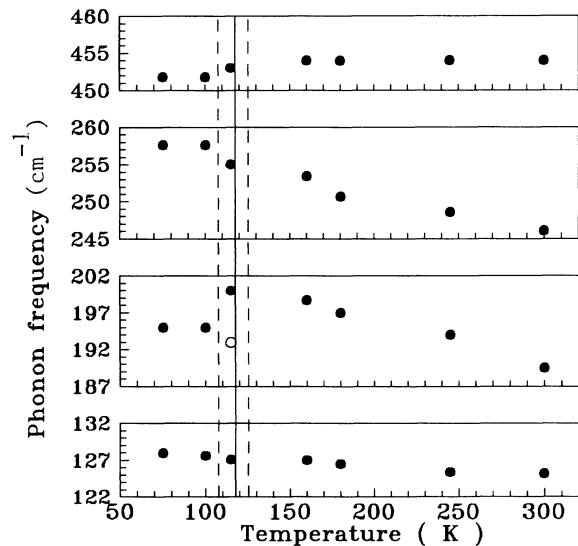


FIG. 5. Dependence of the four A_g mode frequencies with temperature. The vertical line shows the transition temperature and the dashed lines the temperature range of the LTO and LTT phase coexistence. Incident wavelength: 5145 Å.

modes at 190 and 245 cm^{-1} show a quite strong increase of their frequencies when the temperature is decreased towards the LTO-LTT phase transition one. The normal modes depicted in Fig. 2 can also be grouped in two blocks. One is related to the vibrations of the oxygen octahedra around the Ni ions: Figure 2(a) is a rigid rotation, Fig. 2(b) is a deformation of the octahedron, and Figs. 2(c) and (2d) are the stretching modes of the two kinds of oxygens. The second group is formed by the vibrations of the Pr, O(2) layers, Figs. 2(e) and 2(f).

The rigid rotation of the octahedra has the lowest energy, and so it can be assigned to the 125- cm^{-1} peak. The $A_g(b)$ involves Ni-O bond bendings and appears at 322 cm^{-1} and the $A_g(c)$, which is the Ni-O(2) stretching mode, is seen at 450 cm^{-1} as in other related compounds.

On the other hand, the Pr_2O_2 -layer A_g modes are assigned to the 190- and 245- cm^{-1} peaks. The behavior of the 190- cm^{-1} mode, when the temperature is varied from 300 to 40 K, is quite similar to that described by Burns *et al.*⁹ in La_2NiO_4 for a mode at 125 cm^{-1} . Nevertheless, we do not think that it should be ascribed to the same process. They observe, in the La compound at 80 K, a mode at 125 cm^{-1} whose frequency decreases until it reaches the value of 110 cm^{-1} at room temperature, and they assign this peak to the LTO-to-HTT soft mode. Since the transition temperature is around 770 K, it is possible to observe, in the La compound, some dependence of the frequency even in this temperature range (below 300 K). On the other hand, since the LTO-to-HTT phase transition in the Pr compound is around 1500 K, it is then not very probable to observe any softening of a mode associated with this transition when the experiments are done below room temperature. Nevertheless, after the HTT-LTO transition occurs, a continuous deformation has been observed in the 300–117-K range by use of neutron diffraction. The rotation angle of the oxygen octahedra increases when the temperature decreases until the low-temperature phase transition occurs, which implies a different rotation axis. This rotation is rigid during all the process: the Ni-O(1) and Ni-O(2) distances are practically unaffected by changes in the temperature. This explains why the frequencies associated with the octahedra [Figs. 2(a)–2(d)] vary by less than 2 cm^{-1} in 200 K. As a result of this rotation, the Pr-O(2) layers are deformed and the O(2) ions are pushed towards the Pr ions, including an increase in the frequencies of the Pr-O(2) layer modes.

We cannot determine the correspondence between the two modes and the two observed peaks, but, because of their relative intensity, we would assign the more intense (190 cm^{-1}) to the mode that involves basically movements along the c axis [Fig. 2(e)]. As can be seen in Fig. 5, the frequency of the 245- cm^{-1} peak increases up to a saturation value after the low-temperature phase transition, while that of the other peak drops from 200 cm^{-1} at 115 K to 195 cm^{-1} at 100 K. The decrease of this mode frequency points out that the transition is energetically favorable to the deformation associated to this vibration.

Analyzing the shape of the 190- cm^{-1} peak at different temperatures and fitting them to Lorentzian functions, we can unambiguously determine that the peak at 115 K

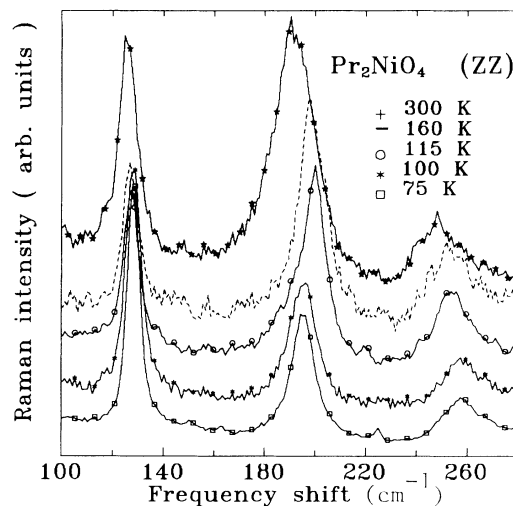


FIG. 6. (zz) Raman spectra at five temperatures showing three A_g modes. The spectra have been shifted vertically. The normalization is done with the 450- cm^{-1} peak (not shown). Incident wavelength: 5145 Å.

contains two Lorentzians (their positions have been indicated in Fig. 5), while at other temperatures one Lorentzian function is enough. Unfortunately, the 245- cm^{-1} peaks are too weak for a similar analysis to be carried out. Figure 6 shows three A_g modes at five temperatures; the incident wavelength in this case was 5145 Å and the spectra were normalized to the 450- cm^{-1} peak intensity. The observation of a double peak in the 115-K spectrum supports the coexistence of the two phases (LTO and LTT) claimed in some structural studies.¹⁹ The range of temperatures, where the two phases coexist is indicated in the Fig. 5 with dashed lines.

B. Magnetic dynamics

In this work we present some results that seem to be better understood in the framework of a quantum spin-fluctuation ground state described for the cuprates than with the original theory developed for the nickelates. The characteristics of the Pr_2NiO_4 single-crystal light scattering associated with magnons are closer to those reported for the copper compounds than for the La_2NiO_4 , as we will describe later.

At room temperature, some weak features are observed in the high-frequency range of the Pr_2NiO_4 spectra. The double phonon peaks of the two kinds of oxygen stretching [in Fig. 7, the O(2) stretching mode is labeled as A and the O(1) mode as B] are seen in their respective configurations. Also, a weak broad band can be observed in the (zz) configuration in the 1500–3000- cm^{-1} region.

When the temperature is stabilized at 75 K, a strong and very broad band appears in the (zz) spectrum. The other two configurations also show bands, though they are much weaker. This strong dependence on the temperature is, in principle, quite surprising, since the sample is already antiferromagnetically ordered at room temperature ($T_{N1} = 325$ K).¹⁹

Following the previously described analysis developed by Lyons *et al.*,²⁴ we have obtained the values of the first three cumulants for the 75-K spectra. Even if the errors are important because of the low intensities and background subtraction problems, we can state with confidence that the obtained values (Table III) do not correspond to the picture valid for the K_2NiF_4 compound. The ratio M_2/M_1 , where M_2 is a measure of the width and M_1 gives the center of gravity of the observed spectrum, is very close to the calculated value²³ (0.23) and to the experimental values found in the La, Nd and Sm cuprates (0.23–0.28).¹⁷ Very recently a direct measure of the exchange J parameter has been obtained by use of inelastic neutron scattering in La_2NiO_4 ,²⁵ the value obtained (248 cm^{-1}) is very close to the one extracted from two-magnon light scattering (240 cm^{-1}).¹⁶ In Pr_2NiO_4 , the value (around 400 cm^{-1}) is probably higher due to the magnetic contribution of the Pr ions. Nevertheless, the cuprates present much higher exchange parameters around $1000\text{--}1200\text{ cm}^{-1}$.

Similar characteristics, of width and shape of the bands, found in Pr_2NiO_4 as in the cuprates seem to indicate that in this case also (with $S=1$) quantum spin fluctuations in the ground state are important (see Fig. 8). However, this theory cannot explain the strong scattering intensity observed in the (zz) configuration. In this sys-

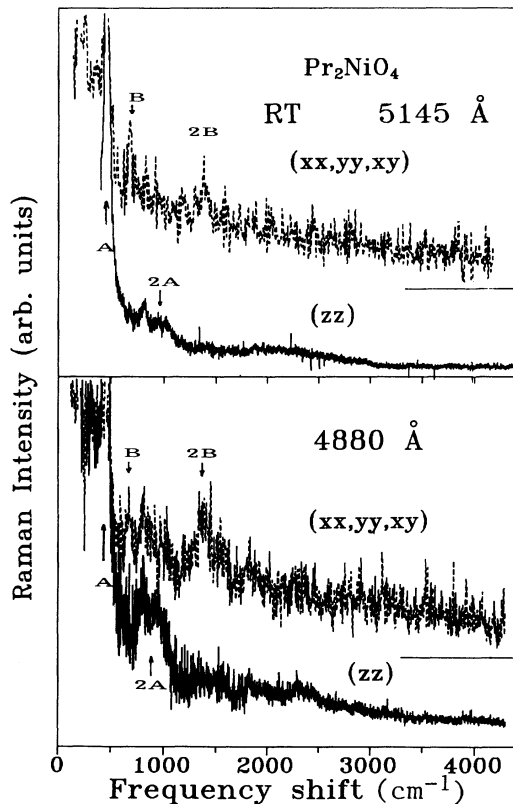


FIG. 7. High-energy zone of the Pr_2NiO_4 Raman spectra with two incident wavelengths and three polarizations. The O(2) stretching mode is labeled as A and the O(1) mode as B. The multiphonons are indicated.

TABLE III. Values of the first three cumulants in the three configurations at 75 K with an incident wavelength of 5145 \AA . The ratios are given in order to compare them to the calculated value (Ref. 23) (0.23) for the quantum spin-fluctuation ground state.

Pr_2NiO_4 75 K	A_{1g} (zz)	$A_{1g} + B_{1g} + B_{2g}$ (xx,xy,yy)	E_g (zx,zy)
M_1 (cm^{-1})	3050	2600	2800
M_2 (cm^{-1})	950	730	680
M_3 (cm^{-1})	750	(300)	(300)
M_2/M_1	0.31	0.28	0.24
J (cm^{-1})	455	388	418

tem the structural low-temperature phase transition has important effects on the magnetic structure, as pointed out before. The LTT structure allows an out-of-plane canting of the Ni magnetic moments, which has been actually observed.²⁰ Moreover, the magnetic phase transition detected around 90 K shows that not only the z component of the Ni moment is large, but that it is also anti-

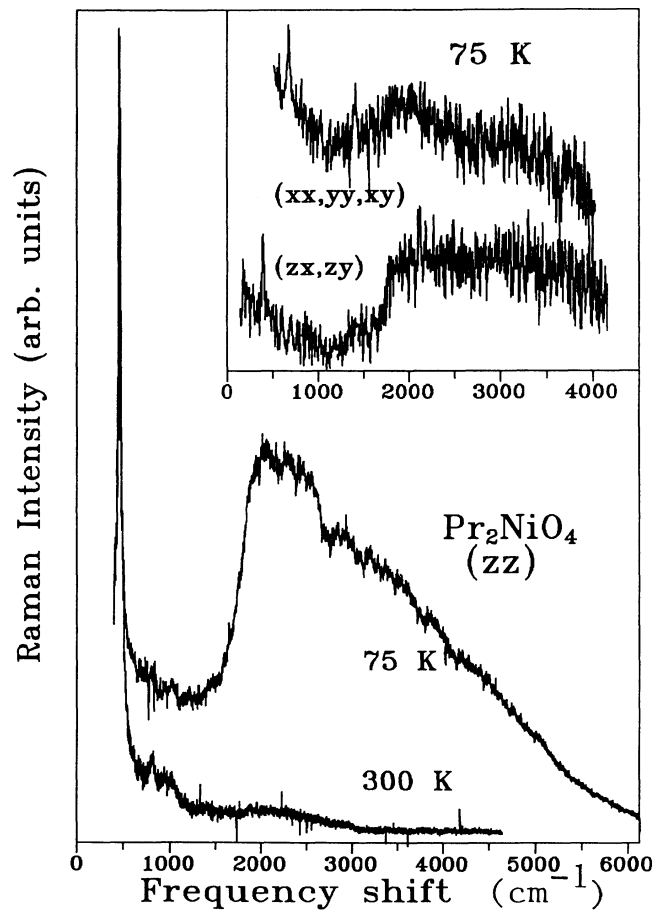


FIG. 8. High-energy zone of the Pr_2NiO_4 (zz) Raman spectra at two temperatures. The intensities have been normalized with the 450-cm^{-1} peak. The inset shows the other two configurations at 75 K; the intensity scale is expanded a factor of 1.5 with respect to the (zz) spectrum. Incident wavelength: 5145 \AA .

ferromagnetically ordered in the direction perpendicular to the layers. This is a clear demonstration that the coupling between the Pr_2O_2 layers is not at all negligible.

When the interlayer magnetic coupling is taken into account, the light scattering from magnons is no longer limited to the Ni-O(1) planes. On the contrary, if the magnetic moment has a component perpendicular to the planes, the configuration with the incident and scattered electric fields parallel to the c axis is expected also to show a band of similar characteristics as in the other configurations. For these reasons, we consider the intensity observed in the (zz) low-temperature spectrum to be related with two-magnon scattering arising from spin flips of Ni ions in two different layers. In this compound the ratio of the interlayer and intralayer Ni nearest-neighbor distances is 1.7, i.e., smaller than for the K_2NiF_4 compound (1.9). The decrease of this ratio means that, in comparison, the Ni ions of consecutive layers are closer in the Pr compound than in the K_2NiF_4 . This partly explains why the interlayer exchange constant has to be taken into account. Moreover, praseodimium ions probably play an important role in this interlayer coupling; in fact, below 40 K, these ions are also AFM ordered and coupled to the Ni magnetic moments.

The reason why the intensities in the (xx), (yy), and (xy) configurations are so low in comparison to that of the (zz) component is not yet clear. There seem to be some screening effects in all the light-scattering processes in this compound.

We have also observed that the (zz) two-magnon band is resonant when the incident wavelength is changed from 4880 to 5145 Å. This resonance also occurs for the 125- and 322- cm^{-1} peaks at 75 K; we have to point out that these two peaks correspond to oxygen octahedra modes. Apparently, a resonance with some electronic level is achieved at the 5145-Å wavelength and a quite strong L - S coupling induces an increase of the scattered

light also in the two-magnon spectrum. This strong interaction has already been deduced in the cuprates.¹

As it is shown, the light scattering arising from the magnetic fluctuations has a quite complicated behavior with temperature and, in fact, the spectra seem to be composed of at least two bands. A more detailed analysis of more extensive experimental data is in progress.

VI. CONCLUSIONS

The main conclusions of this study are the following: Concerning the lattice vibrational modes of the LTO phase, the A_g phonons have a zz coefficient much higher than the others (xx, yy) and the correspondence with particular atomic displacements is found. Among the other allowed modes, some have been identified but others seem to be very weak. The number of first-order modes is not higher than that predicted by point-group analysis, in contrast with what other authors have found in some cuprates. Several multiphonon bands have been detected, which correspond to higher orders of the two oxygen stretchings. The LTO-to-LTT phase transformation has been followed. In the tetragonal phase, three additional modes are detected instead of the five expected. The dependence of the frequencies with the temperature gives us a basis for the assignation of some modes and also shows the coexistence of both phases near the transition temperature, in particular at 115 K.

With respect to the magnetic behavior of the sample, two-magnon light scattering has been detected clearly at 75 K with the highest intensity in the (zz) configuration. The characteristics of the spectra do not correspond to those expected from the two-magnon scattering, even including magnon-magnon interactions. Interlayer magnetic coupling of the Ni ions must be taken into account in this compound in order to explain the present experimental results.

¹S. Sugai, Phys. Rev. B **39**, 4306 (1989).

²S. Sugai, S. Shamoto, M. Sato, T. Ido, H. Takagi, and S. Uchida, Solid State Commun. **76**, 371 (1990).

³F. Gervais, P. Echegut, J. M. Bassat, and P. Odier, Phys. Rev. B **37**, 9364 (1988).

⁴A. V. Bazhenov, T. N. Fursova, V. B. Timofeev, A. S. Cooper, J. P. Remeika, and Z. Fisk, Phys. Rev. B **40**, 4413 (1989).

⁵R. J. Birgeneau, C. Y. Chen, D. R. Gabbe, H. P. Jenssen, M. A. Kastner, C. J. Peters, P. J. Picone, T. Thio, T. R. Thurston, H. L. Tuller, J. D. Axe, P. Böni, and G. Shirane, Phys. Rev. Lett. **59**, 1329 (1987); P. Böni, J. D. Axe, G. Shirane, R. J. Birgeneau, D. R. Gabbe, H. P. Jenssen, M. A. Kastner, C. J. Peters, P. J. Picone, T. R. Thurston, Phys. Rev. B **38**, 185 (1988).

⁶T. R. Thurston, R. J. Birgeneau, D. R. Gabbe, H. P. Jenssen, M. A. Kastner, P. J. Picone, N. W. Preyer, J. D. Axe, P. Böni, G. Shirane, M. Sato, K. Fukuda, and S. Shamoto, Phys. Rev. B **39**, 4327 (1989).

⁷N. Ogita, M. Udagawa, K. Kojima, and K. Ohbayashi, J. Phys. Soc. Jpn. **57**, 3932 (1988).

⁸J. M. Bassat, P. Odier, and F. Gervais, Phys. Rev. B **35**, 7126

(1987).

⁹G. Burns, F. H. Dacol, D. E. Rice, D. J. Buttrey, and M. K. Crawford, Phys. Rev. B **42**, 10777 (1990); D. E. Rice, M. K. Crawford, D. J. Buttrey, and W. E. Farneth, *ibid.* **42**, 8787 (1990).

¹⁰F. Bates and J. E. Eldridge, Solid State Commun. **72**, 187 (1989).

¹¹L. Pintchovius, J. M. Bassat, P. Odier, F. Gervais, G. Chevrier, W. Reichardt, and F. Gompf, Phys. Rev. B **40**, 2229 (1989).

¹²A. De Andres, M. T. Fernandez-Diaz, J. L. Martinez, J. Rodriguez-Carvajal, R. Saez-Puche, and F. Fernandez, J. Phys.: Condens. Matter **3**, 3813 (1991).

¹³A. De Andres, M. T. Fernandez-Diaz, J. L. Martinez, J. Rodriguez-Carvajal, R. Saez-Puche, and F. Fernandez, Euro. J. Solid State Inorg. Chem. **28**, 179 (1991).

¹⁴F. Fernandez, R. Saez-Puche, M. T. Fernandez-Diaz, J. Rodriguez-Carvajal, J. L. Martinez, I. L. Botto, and E. J. Baran, Euro. J. Solid State Inorg. Chem. **28**, 507 (1991).

¹⁵S. Sugai, T. Kobayashi, and J. Akimitsu, Phys. Rev. B **40**, 2686 (1989).

- ¹⁶S. Sugai, M. Sato, T. Kobayashi, J. Akimitsu, T. Ito, H. Takagi, S. Uchida, S. Hosoya, T. Kajitani, and T. Fukuda, *Phys. Rev. B* **42**, 1045 (1990).
- ¹⁷P. E. Sulewski, P. A. Fleury, K. B. Lyons, S-W. Cheong, and Z. Fisk, *Phys. Rev. B* **41**, 225 (1990).
- ¹⁸R. Saez-Puche, F. Fernandez, J. L. Martinez, and J. Rodriguez-Carvajal, *Solid State Commun.* **72**, 273 (1989).
- ¹⁹J. L. Martinez, M. T. Fernandez-Diaz, J. Rodriguez-Carvajal, and P. Odier, *Phys. Rev. B* **43**, 13 766 (1991); also M. T. Fernandez *et al.* *Z. Phys. B* **82**, 275 (1991).
- ²⁰J. L. Martinez *et al.* (private communication).
- ²¹J. B. Parkinson, *J. Phys. C* **2**, 2012 (1969).
- ²²P. E. Fleury and H. J. Guggenheim, *Phys. Rev. Lett.* **24**, 1346 (1970).
- ²³R. R. P. Singh, P. A. Fleury, K. B. Lyons, and P. E. Sulewski, *Phys. Rev. Lett.* **62**, 2736 (1989).
- ²⁴K. B. Lyons, P. A. Fleury, R. R. P. Singh, and P. E. Sulewski, in *Dynamics of Magnetic Fluctuations in High Temperature Superconductors*, edited by G. Reiter (Plenum, New York, 1991), p. 159.
- ²⁵K. Yamada, M. Arai, Y. Endoh, S. Hosoya, K. Nakajima, T. Perring, and A. Taylor, *J. Phys. Soc. Jpn.* **60**, 1197 (1991).